Contents lists available at ScienceDirect

International Journal of Multiphase Flow
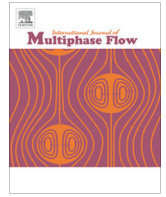
Experimental evaluation of conductive flow imaging using magnetic induction tomography

CrossMark

Lu Ma [a,1], Andy Hunt [b,2], Manuchehr Soleimani [a,*]

[a] Engineering Tomography Laboratory (ETL), Department of Electronic and Electrical Engineering, University of Bath, Bath BA2 7AY, UK
[b] iPhase Ltd, Unit 6, New Forest Enterprise Centre, Chapel Lane, Totton SO40 9LA, UK

ABSTRACT

Multi-phase flow imaging is a challenging topic in industrial process tomography. In this paper, we present a non-invasive imaging technique for the electrically conductive phase of a multi-phase flow problem. Magnetic induction tomography (MIT) is sensitive to the conductivity of the target, and as such has the potential to be used as an imaging technique to visualise the conductive components in a multi-phase flow application. A 16 channel MIT system is used for this study, among which eight excitation coils are supplied with a 15 V peak, 13 MHz sinusoidal signal in sequence from a signal generator, while the remaining eight coils are floated as receivers. The imaging region of this MIT system has an inner and outer diameter of 190 mm and 200 mm respectively. Static fluid distribution patterns are produced using several fluids with different conductivities and placed inside the imaging region to form conductivity phase contrasts. Experimental results show within our hardware and software capability, a conductivity contrast of 0.06 S/m for an inclusion that occupies 8.69% of the imaging region can be imaged. An in-depth experimental evaluation of the system response towards various fluid measurements is shown for the first time, as are results for quasi-static fluid experiments showing that a non-homogenous flow of gas bubbles can be imaged in various conductive backgrounds. In sum, the analyses presented investigate the feasibility and capability of MIT for this application, while also reporting some of the first flow rig tests in this field.

© 2015 Elsevier Ltd. All rights reserved.

Introduction

Magnetic Induction Tomography (MIT) is also known as electromagnetic induction tomography or eddy current tomography. It is a relatively low cost technique, although due to its soft-field nature, the resolution of MIT has not yet met the standards for widespread commercialisation. The underlying principles of MIT is that a magnetic field is excited and registered by inductive coils arranged around the imaging region; the spatial distribution of magnetic field and the mutual coupling between the coils is then altered by material presented in the imaging region. Materials can be either ferromagnetic or conductive. In a typical 2D phantom study case, the cross-sectional images of the properties of the object can be reconstructed using the voltage or phase measurements collected from the inductive coils. Because of the non-hazardous, non-invasive

and contactless natures of MIT, its use has been proposed for numerous applications, including foreign material monitoring (Daily and Ramirez, 1995), geological exploration (Griffiths, 2001), non-destructive evaluations (Ma and Soleimani, 2012; Yin and Peyton, 2006; Renner et al., 2012), and biomedical imaging (Griffiths et al., 1999; Scharfetter et al., 2001; Ma et al., 2012; Peyton et al., 2003; Korzhenevsky and Sapetsky, 2001; Karbeyaz and Gencer, 2003; Rosell-Ferrer et al., 2006; Igney et al., 2005; Watson et al., 2002).

It is also considered more advantageous to use MIT in flow imaging compared to electrical resistance tomography techniques (Jin et al., 2013; Su et al., 2013; Zhang and Ma, 2013). Due to the low resolution of this technique, the realisation of MIT as a smart imaging device for industrial process tomography remains a challenging topic. There have been reported cases where MIT is used for metal visualisation and solidification (Ma et al., 2006; Ma et al., 2008; Terzija et al., 2011); however, the experimental validation in two-phase or multi-phase flow imaging using MIT is still limited. It is considered that MIT could be complementary to existing techniques for multi-phase flow imaging as MIT is sensitive to the conductive component of the flow mixtures (Thorn et al., 2013; Zhang et al., 2014). A feasibility study of electromagnetic imaging

* Corresponding author. Tel.: +44 01225 386310.
    E-mail addresses: lu.ma@bath.edu (L. Ma), andyhunt@iphaseflow.com (A. Hunt), m.soleimani@bath.ac.uk (M. Soleimani).
[1] Tel.: +44 01225 386310.
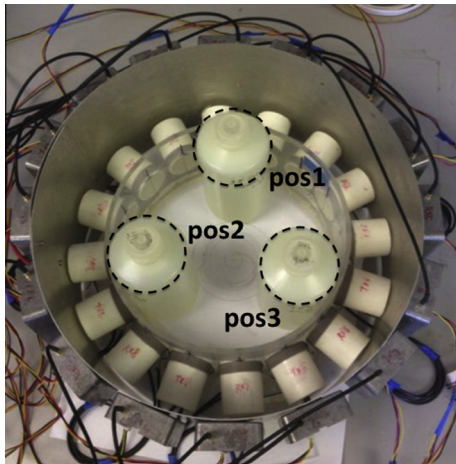[2] Tel.: +44 (0) 23 8178 2922.

Fig. 1. The experimental setup, in this case showing three inclusions within the imaging region.

in distinguishing two type of conductivities: fat and water-bearing fat free tissues was presented in 1993 (AL-Zeibak and Saunders, 1993). This study was primarily focused on the imaging of biomedical tissue, however, the concept of MIT be used in flow process was introduced and validated for the first time. Albrechtsen et al. (1995) proposed a single channel MIT system to measure the water content in multi-phase flow using experimental phantom recordings. Based on the observations, the authors concluded the correlation between the position of the coil and the water/oil interface could be overcome by a full tomographic system. Similar conclusions have also been drawn by Hammer and Fossdal (2002). Liu et al. (2005) proposed a parallel excitation structure for MIT in an attempt to image conductive or ferromagnetic properties in two phase flow. However, this work was limited in scope, focussing a simulation of the sensing field, and as such experimental results were not included in the publication. It was not until 2008 that a full MIT system had demonstrable feasibility for two phase flow imaging. Watson et al. (2008) studied a phantom simulated multiphase flow in an oil pipeline, with the imaging conductivity of the
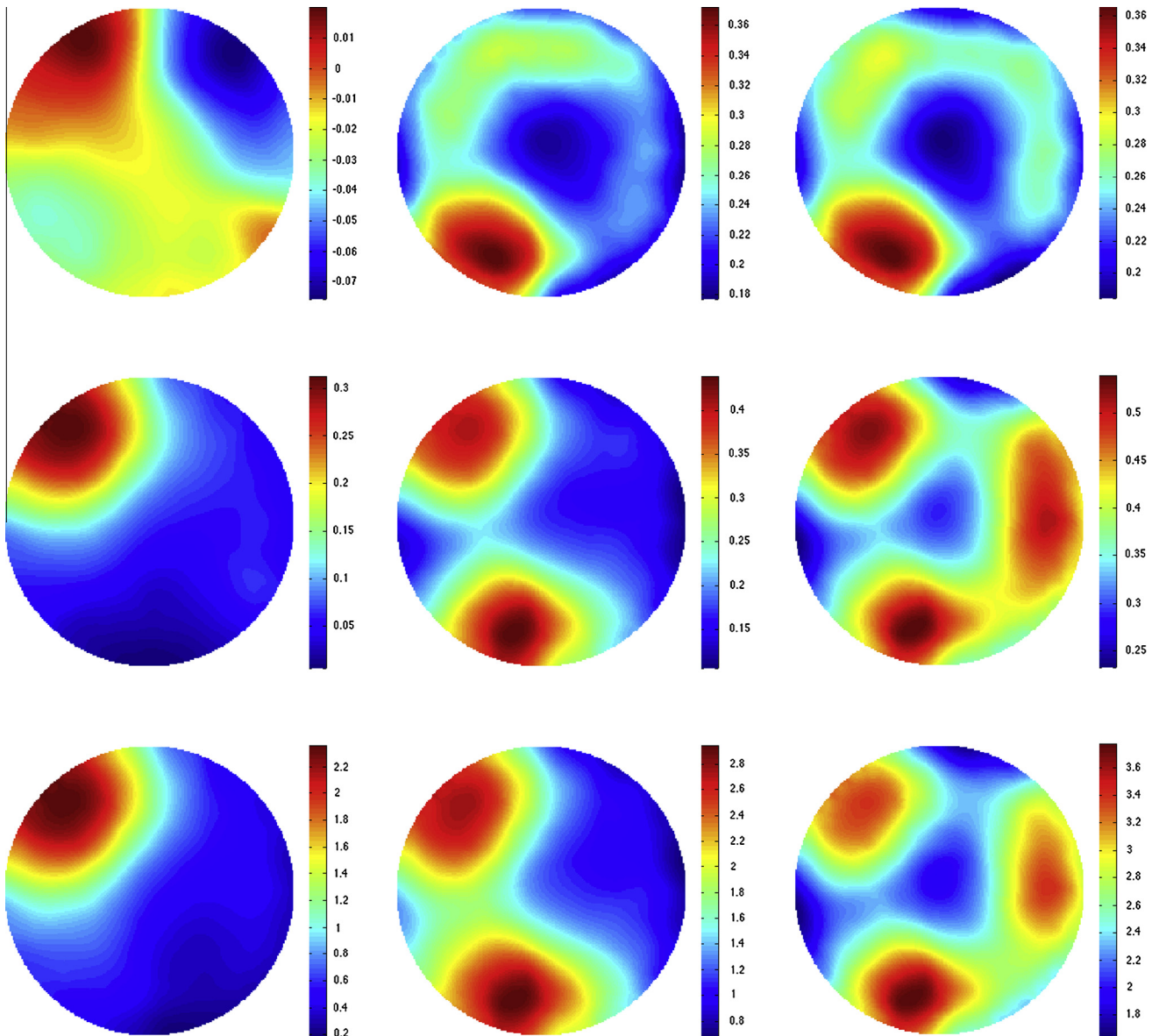

Fig. 2. Reconstructed images for, by row, small, medium and large inclusions of, by column, one, two and three inclusions in a free space background. The conductivity of the inclusion is 1.52 S/m in all cases.

system found to be below 10 S/m. More recently, Wei and Soleimani (2012) demonstrated an experiment-based two phase flow imaging using a 16 channel MIT system.Although the experimental results were satisfactory, showing that a conductivity contrast as small as 1.58 S/m can be imaged, the authors did not pursue further analysis of the results.

This paper presents a critical evaluation of MIT for two phase flow imaging. Both static and quasi-static experiments are presented to evaluate the MIT in variety of conditions. The practical difficulties, fundamental limitation, and potential improvement of this technique are discussed.

Method

In a MIT system, the coil array consists of a set of excitation coils, which produce an electromagnetic field within a cross section of an imaging region. A set of detection coils are used to detect the changes in the field due to changes in permeability and conductivity inside the vessel. The governing equations of MIT problem are as follows.

$$\nabla \times E = -j\omega\mu H \tag{1}$$

$$\nabla \times H = (\sigma + j\omega\varepsilon)E \tag{2}$$

$$\nabla \cdot \mu H = 0 \tag{3}$$

where ∇ is the gradient operator, E is the electric field strength, H is the magnetic field strength, ω is the applied angular frequency, μ is the magnetic permeability, σ is the electrical conductivity and ε is the permittivity distribution in the sensing field. In the forward problem of MIT, a reduced magnetic vector potential is used (Biro, 1999). The general equation in quasi-static electromagnetic field can be written as Eq. 4.

$$\nabla \times \frac{1}{\mu}\nabla \times A_r + j\omega\sigma A_r = \nabla \times H_s - j\omega\sigma A_s - \nabla \times \frac{1}{\mu}\mu_0 H_s \tag{4}$$

where A_r is the reduced magnetic vector potential in the eddy current region, where H_s is the magnetic field generated by an excitation coil, which can be directly computed from in any point P in free space from source current density J_s:

$$H_s = \int_{\Omega_n} \frac{J_s(Q) \times r_{QP}}{4\pi|r_{QP}|^3} d\Omega_Q \tag{5}$$

where r_{QP} is the vector pointing from the source point Q to the field point P. A_s is the impressed magnetic vector potential as a result of
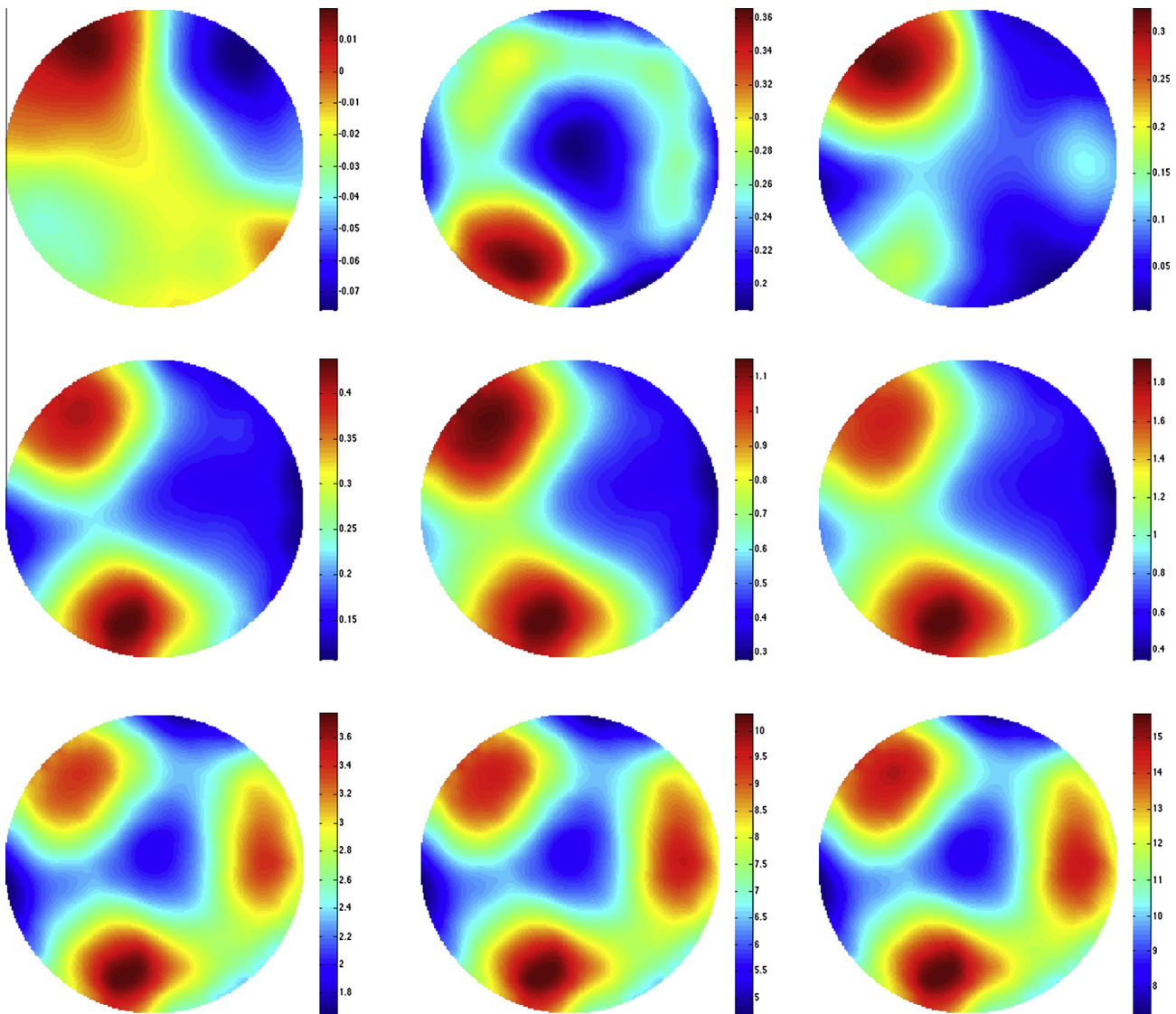

Fig. 3. Reconstructed images for, by row, one, two and three inclusions of, by column, small, medium and large inclusions in a free space background. The conductivity of the inclusion is, by column, 1.52 S/m, 4.06 S/m and 5.94 S/m respectively.

J_s, and μ_0 is the permeability of the free space. In Eq. 4, the only unknown is A_r, which can be computed by solving the system linear equation (Soleimani and Lionheart, 2006).

$$SA_r = b \qquad (6)$$

where S is a system matrix, and b is the right hand side current density. The inverse problem of MIT can be solved by using a linear image reconstruction algorithm (Hu et al., 2007).

$$\Delta\sigma = \left(J^T J + \alpha R_1 + \beta R_2\right)^{-1} J^T (\Delta V) \qquad (7)$$

where ΔV is the change in the induced voltage measurements, J is the sensitivity matrix computed from the forward model (Widlak and Scherzer, 2012), R_1 is a Laplacian regularisation term, R_2 is an identity matrix, and α and β are the regularisation factors for R_1 and R_2 respectively. As shown in 7, this linear image reconstruction algorithm utilises a combination of Laplacian and Tikhonov based
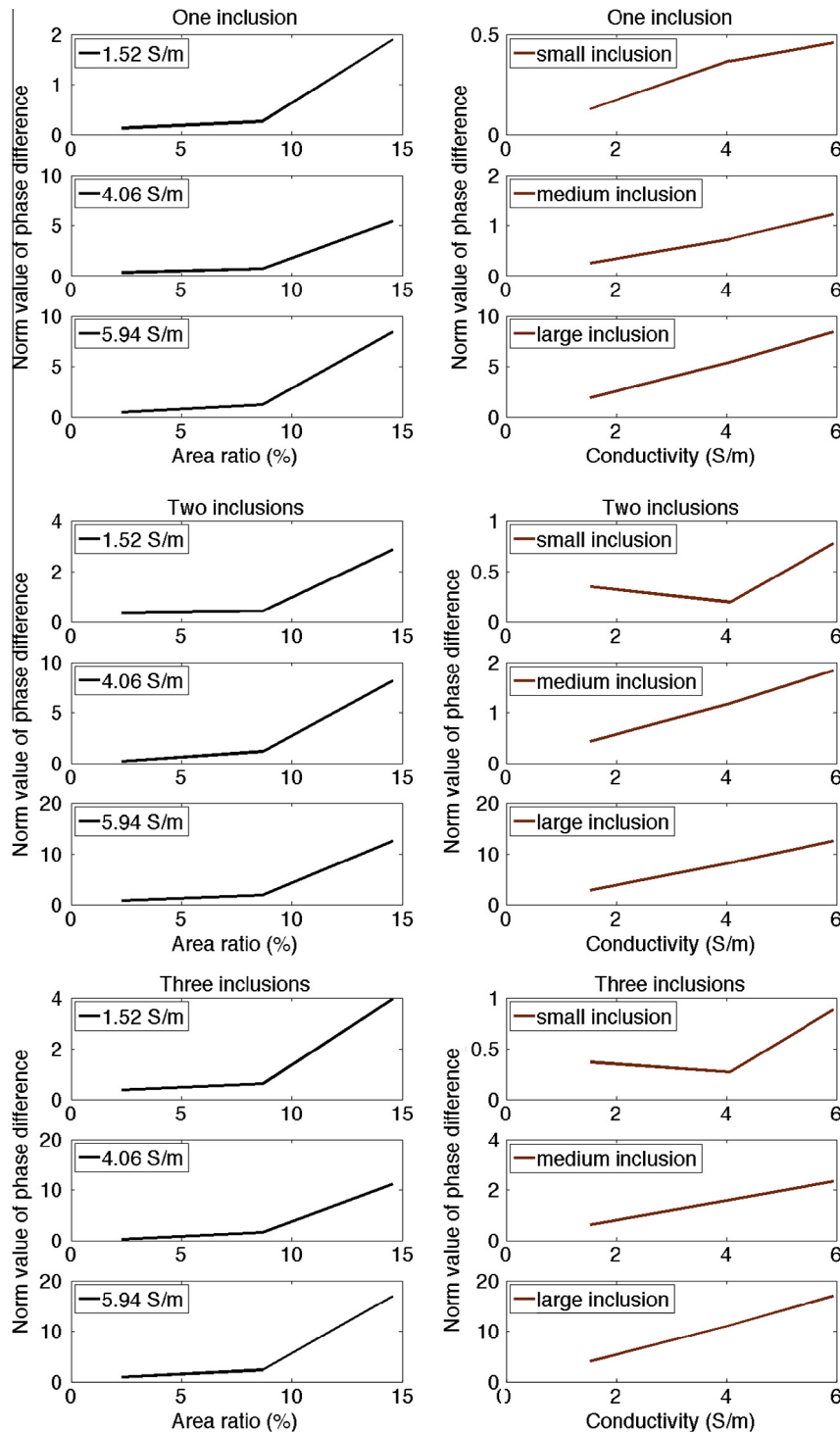

Fig. 4. The norm value of the phase difference against the change in area ratio (left, in black) and the change in conductivity level (right, in brown). Both sets of plots are produced using one, two or three inclusions (top to bottom, respectively). (For interpretation of the references to color in this figure legend, the reader is referred to the web version of this article.)

regularisation terms, therefore it is also called hybrid reconstruction algorithm. This algorithm is found to be effective, particularly in cases whereby there is a non-uniform distribution of the sensitivity map in the imaging region (Chen et al., 2008; Lu et al., 2008); however, it is not a well established algorithm in terms of selecting the regularisation parameters automatically. In this study, the regularisation parameters are selected empirically, with the values $\alpha = 1e - 3$ and $\beta = 1e2$. Both parameters are applied to reconstructed the images presented throughout the paper so that the results can be compared in a fair and consistence manner, this is further discussed in later section. It is shown that using this hybrid image reconstruction algorithm, an improved imaging resolution can be achieved compared to using a single regularisation parameter based linear reconstruction algorithm (Wei and Soleimani, 2012).

Static fluid test results

Experimental setup

The Bath MIT system is used for this study, which consists of 16 coils arranged around the imaging periphery. The inner diameter, outer diameter and the length of the imaging region are 190 mm,

200 mm and 90 mm respectively. The driving frequency is 13 MHz, with a 15 V peak driving voltage and a driving current of 0.39 A, the coil resonance frequency is 45 MHz. This system is developed using a series of National Instrument hardwares (Wei and Soleimani, 2012). This system can achieve an imaging speed at approximately 15s per frame. Despite the fact it has not yet met the industrial standard for flowing imaging, it is however suitable for a range of static and quasi-static fluid testing in a laboratory environment.

A series of systematic experiments are conducted to demonstrate the likely conditions of an industrial process environment using static fluid distribution patterns. Several terms are used throughout this study, hence it is worth giving the description for each term.

- Imaging region: the region of interest where the static fluid distribution pattern is measured using 16 inductive coils on the periphery.
- Background conductivity: the conductivity of the contents of the imaging region, excluding any inclusions.
- Inclusion: an area of differential conductivity within the imaging region, as compared to the background conductivity. As this study utilises fluids, the background material and the
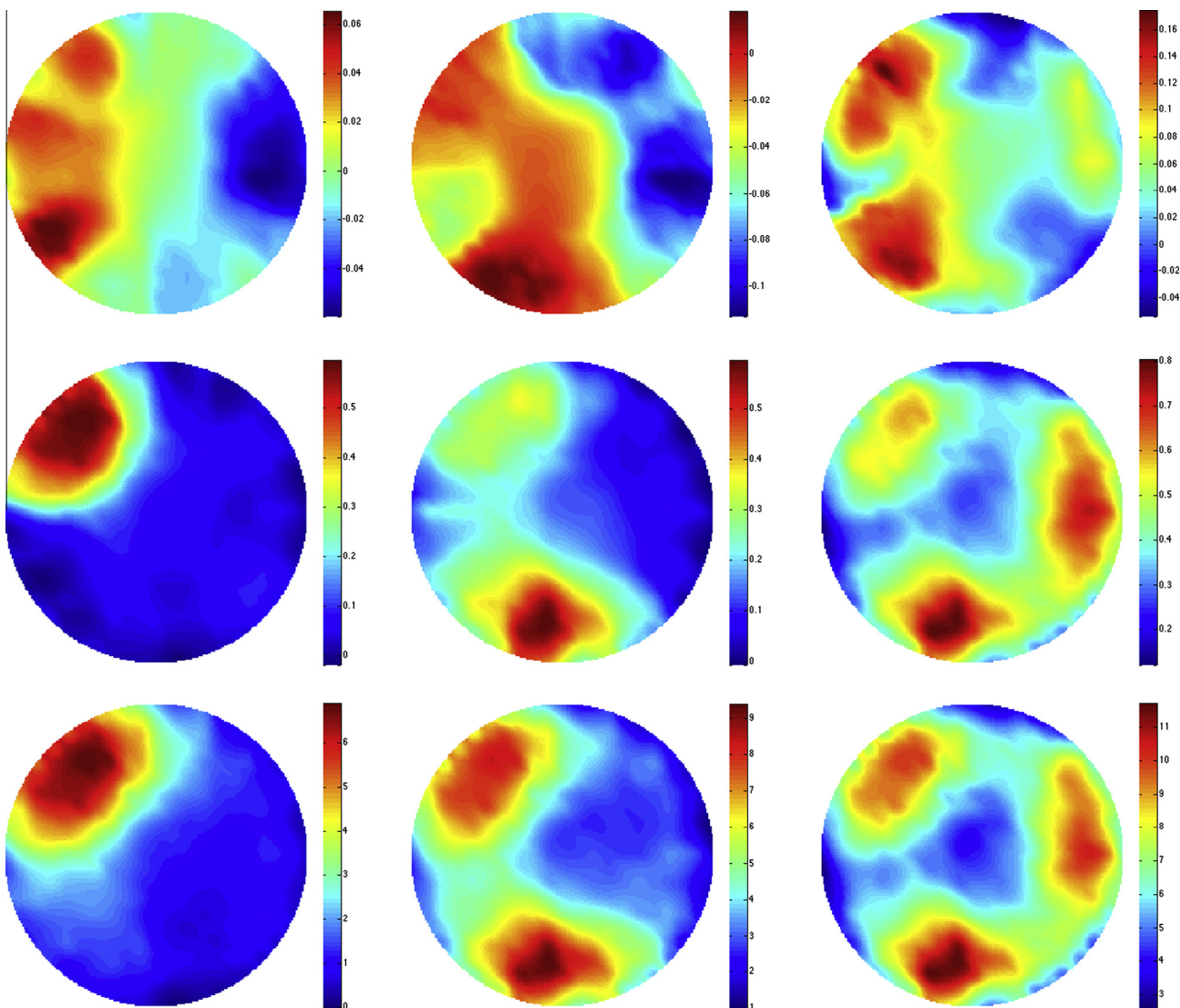

Fig. 5. Reconstructed images for, by row, small, medium and large dimensions of, by column, one, two and three inclusions of saline solution in a free space background. The conductivity of the saline solution is 1.52 S/m in all cases.

inclusion(s) of interest can both be fluid distribution patterns. In this case, the inclusion is kept distinct from the background by being bottled in a non-conductive object.

- Conductivity contrast: the difference between the conductivity of the background and the inclusion.
- Area ratio: ratio of the cross-sectional area of the inclusion to the area of the total imaging region.
- Norm value of phase difference: the norm value of the phase shift measurement between the background and the inclusion (millidegrees), and it is calculated directly from the raw measurements with no calibration. As a difference imaging is used in this study, the norm value presents the phase shifts in a single value.
- Imaging contrast: the ability to distinguish conductivity contrast in an image.
- Imaging resolution: the ability to distinguish between two adjacent structures in an image.

Two scenarios are considered to demonstrate the conductivity contrasts in the imaging region, i.e., conductive inclusion(s) in a non-conductive background and non-conductive inclusion(s) in a conductive background. A static fluid distribution pattern is introduced to the background by bottling the fluid in a non-conductive cylindrical container. In each scenario, the inclusion is measured in three dimensions (28.70 mm, 56.00 mm, and 72.52 mm, hereafter small, medium and large respectively). As the fluid is bottled in a closed area in the imaging region, it is feasible to calculate the ratio of the cross-sectional area of the inclusion to the total imaging region (i.e., area ratio). The area ratios of a single inclusion in the imaging region for small, medium and large dimensions are 2.28%, 8.69% and 14.57% respectively. For each experiment, both single and multiple inclusions of the same size are tested. In the case of a single inclusion, the experiment is conducted in three different positions to assess the spatial homogeneity of the system response (marked as pos1, pos2 and pos3 in Fig. 1). Similarly, when two inclusions are tested in the imaging region, pos1 and pos2 are selected as a representative example; when three inclusions are tested, all three positions are used (Fig. 1). In total, over 600 sets of experiments are conducted to evaluate the MIT system for imaging two phase distributions of static fluid in the imaging region.
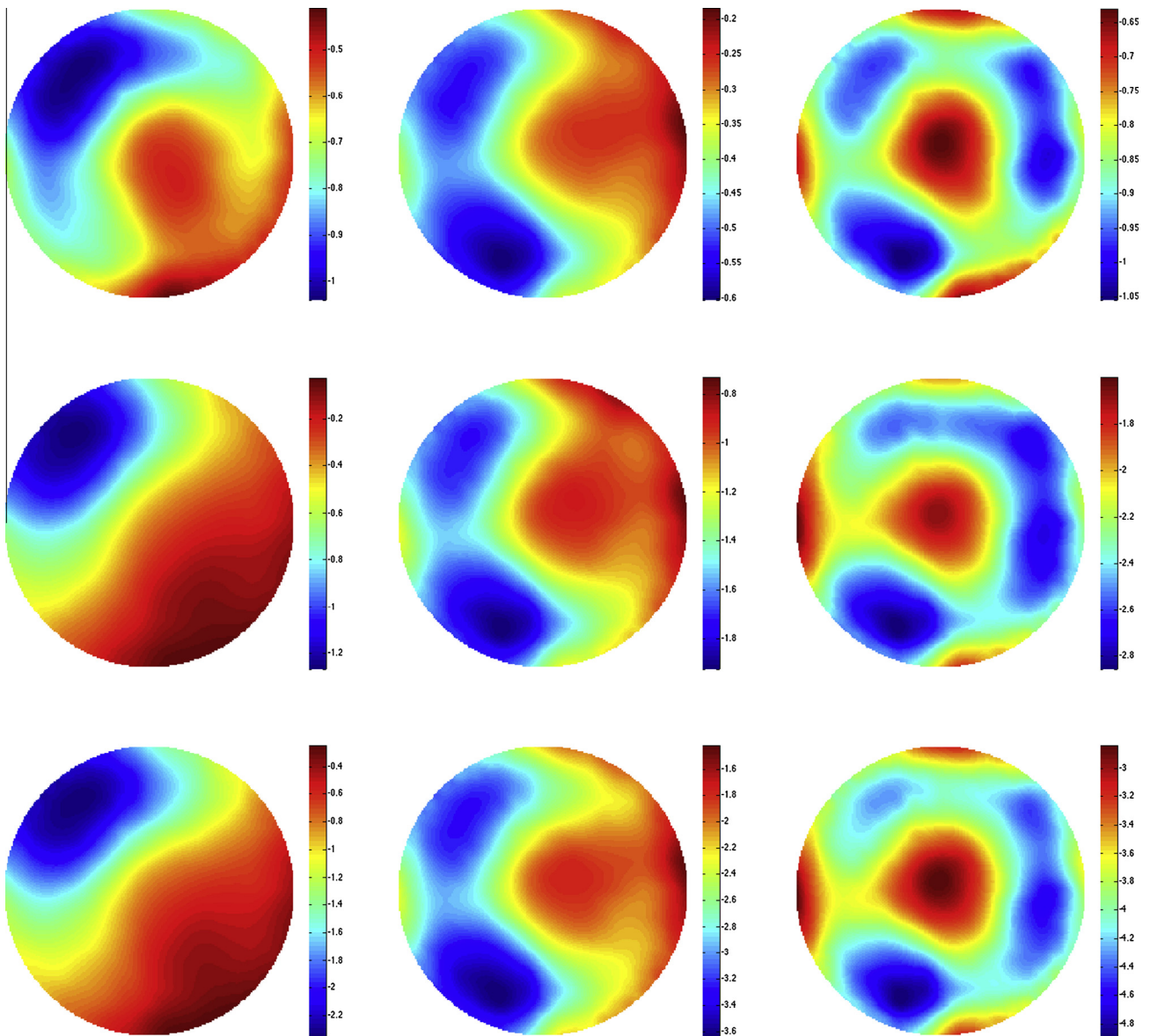

Fig. 6. Reconstructed images for, by row, small, medium and large dimensions of, by column, one, two and three inclusions of silicone oil in a saline solution background (conductivity 1.52 S/m).

The aim of the static fluid distribution tests is to identify the smallest conductivity contrast that can be reconstructed and the area ratio for that contrast.

Fluid distribution patterns in a free space background

Three saline solutions with different conductivity values are used, of 1.52 S/m, 4.06 S/m and 5.94 S/m (low, medium and high) respectively. Each solution is bottled in the aforementioned non-conductive containers (small, medium and large). These containers are placed within the imaging region in each experiment as the only inclusion.

Fig. 2 shows the reconstructed images for, by row, one, two and three inclusions of, by column, small, medium and large area ratios. In all cases, the conductivity of the inclusion(s) is 1.52 S/m. It can be seen that for small inclusions, conductivity contrasts cannot be reliably reconstructed regardless of the position of the inclusion or the number of inclusions in the imaging region (first row in Fig. 2). For both medium and large inclusions, images of one, two or three inclusions can be reliably reconstructed. This suggests that in this scenario, for a given conductivity contrast, if the inclusion cannot be imaged, increasing the number of inclusions does not contribute to any significant gain in information.

However, by increasing the dimension of the inclusion, this could result in an improved resolution in the reconstructed image. This suggests that in this case, the dimension of the inclusion is more informative with regard to image reconstruction than the number of inclusions being imaged. This phenomenon can be explained by reference to the sensitivity distribution of the MIT system: areas nearer sensors are comparatively more sensitive than regions farther away (Soleimani, 2006). Furthermore, although the area ratio covered by a small inclusion is, by definition, less than that of a medium or large inclusion, and increasing the number of inclusions further introduces a field perturbation into the imaging region, small inclusions still cover a less sensitive area compared to medium or large counterparts, resulting in unsuccessful image reconstruction.

In this section, the aim of the experiments is to investigate whether for the same number of inclusions, of the same dimension and at the same testing positions, the conductivity of the inclusion affects its detectability. The first row in Fig. 3 shows the reconstructed images for a single inclusion in the same testing position for conductivities of 1.52 S/m, 4.06 S/m and 5.94 S/m (low, medium and high) respectively. Each column refers to a different inclusion size (small, medium or large). It can be seen that for a single, individual inclusion, an image cannot be reconstructed for at low
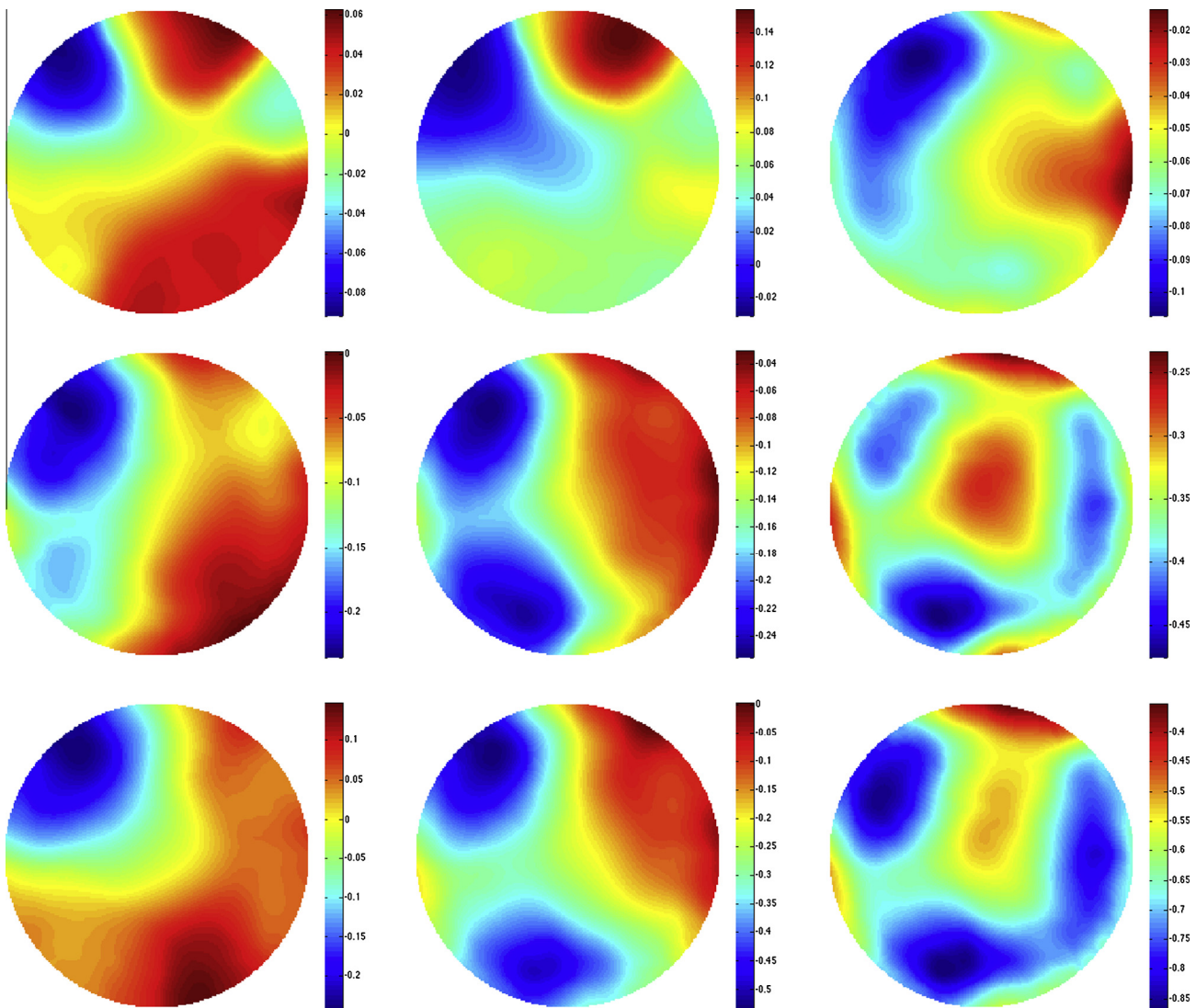

Fig. 7. Reconstructed images for, by row, small, medium and large dimensions of, by column, one, two and three inclusions of silicone oil in a tap water background (conductivity 0.06 S/m).

or medium conductivities and that at high conductivity, the reconstructed image contains multiple, notable artifacts. For two or three inclusions, at all three levels of conductivity, the image reconstructions are successful. By comparing the reconstructed images of multiple medium and multiple large inclusions, we observe more uniform colouration (i.e., similar values) amongst medium-sized compared to large inclusions.

Fig. 4 contains two sets of plots, showing the norm value of the phase difference against either the change in area ratio (left, in black) or the change in conductivity level (right, in brown). Both sets of plots are produced using one, two or three inclusions (top to bottom, respectively). The norm value of the phase difference against the change in area ratio behaves similarly in all cases: there is a low variance for the size change from small to medium, increasing substantially when the dimensions change from medium to large. This is consistent with the results shown in Fig. 2. By contrast, for medium and large inclusions, there is a linear correlation between conductivity level and the norm value of the phase difference. For small dimension, the plots for one, two and three inclusion(s) are inconsistent, this also explains the unsuccessful image reconstruction shown in the top row of Fig. 2.

Fluid distribution patterns in a silicone oil background

The silicone oil used in this study has an electrical insulation property, and as such can be used as a non-conductive background. Fig. 5 shows the reconstructed images of one to three inclusions of a 1.52 S/m saline solution in a silicone oil background (columns left to right, respectively), of either small, medium or large dimensions (first, second and third rows, respectively). We show that the
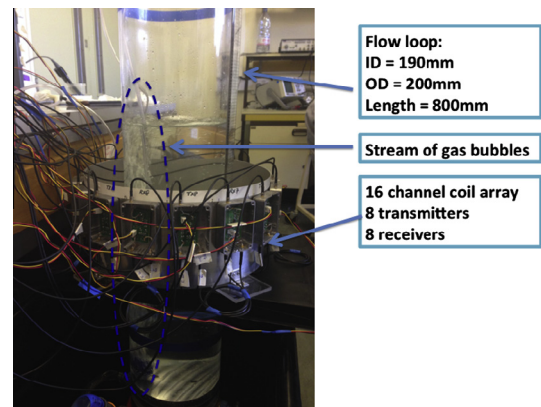

Fig. 9. Bubble testing setup.

image quality increases as the dimension of the inclusion increases, and that furthermore the ability to distinguish the location of multiple inclusions become more pronounced as their dimensions increase.

Fluid distribution patterns in a saline solution background

In this section, two phase liquid imaging is investigated using silicone oil to represent a non-conductive inclusion and saline solution (conductivity 1.52 S/m) as a conductive background. Fig. 6 shows the reconstructed images of three sizes of inclusions – small, medium and large, as shown in the first, second and third

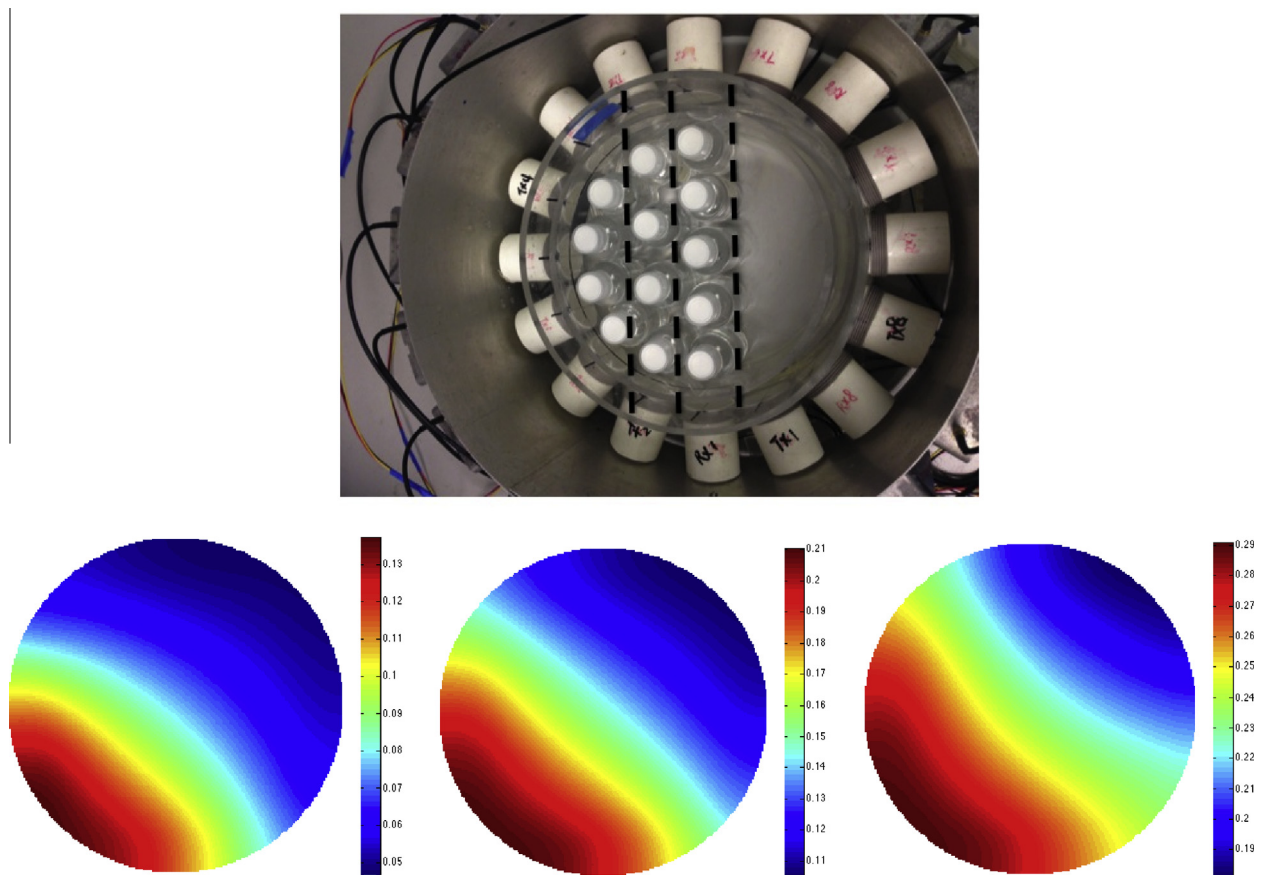

Fig. 8. Experimental setup (top) and reconstructed images (bottom) of three strata, each of non-homogeous conductive fluids in a free space background. By volume, strata are 200 ml, 400 ml and 650 ml, from the left to the right respectively.

rows, respectively. Although the conductivity contrast is the same as presented in Fig. 5, the reconstructed images notably differ. For instance, it appears that the dimension of the inclusion carries comparatively little informative weight with regard to the quality of the image – this is in contrast to Fig. 5, whereby increases in inclusion size from small to medium can noticeably isolate the area of interest.

Fluid distribution patterns in a tap water background

Compared to the other conductive fluids previously discussed, tap water is not only more common but has comparatively low conductivity. As such, we repeated the above experiment using tap water as a background and silicone oil as an inclusion, in order to determine the smallest conductivity contrast at which image reconstruction is still feasible. Fig. 7 shows the reconstructed images of one, two and three inclusion(s) of silicone oil in a tap water background. Although image quality is poor in comparison to previous results, this is nevertheless an encouraging finding, as it shows that image reconstruction is possible at a conductivity contrast of 0.06 S/m, for an inclusion that occupies 8.69% of the total imaging region.

Non-homogenous conductive fluid imaging in a free space background

A stratified flow regime is one of the classic flow regimes in industrial process tomography. A core aspect of this regime is the differentiation of multiple liquid flows, of variable conductivity, into strata. Our experimental setup does not allow the direct testing of flow, although it is nevertheless of interest to determine whether strata can be distinguished for non-homogenous, albeit in this case static, liquids. The aim of this experiment is to study the capability of our system in resolving areas of non-uniform distributions of conductive inclusions. In this experiment, a conductive fluid is used with a conductivity of 6.20 S/m. This fluid is bottled in plastic containers with outer diameter of 37 mm and a height of 79 mm. Each container is fully filled with 50 ml fluid. Strata are created within the imaging region by aligning multiple containers as shown in Fig. 8 (marked by dashed lines). As the conductivity and volume of fluid in each bottle is constant, varying the number of bottles allowed us to vary the total volume of conductive fluid in each stratum. As the bottles are surrounded by free space, each strata is a non-homogenous mix of both conductive and non-conductive material. Three strata are tested, varying by total volume of conductive fluid (4, 8, and 13 containers, i.e., 200 ml, 400 ml and 650 ml, respectively). Reconstructed images shown from the left to the right in the bottom row of Fig. 8.

Quasi-static fluid measurements

This section investigates the feasibility of gas bubble imaging in a flow rig. The inner diameter, outer diameter and the length of the flow rig are 190 mm, 200 mm and 800 mm respectively. The flow rig is positioned centrally in the imaging region with a 16 channel coil array on the periphery (Fig. 9).

Five different conductive fluids are used in this experiment, with conductivities of 0.06 S/m, 1.81 S/m, 3.20 S/m, 5.13 S/m and 12.64 S/m respectively. The background data are taken from the empty flow rig, and the fluid measurements are taken when the flow rig is filled with different volumes of fluids, from 4, 6, 7, 8, 9, 10, 11, 12, 13 to 15 litres. Repeated measurements are also taken as the rig is drained. The aim of these tests is to assess both the sensitivity of the system, and the optimal range of conductivity range that can be accurately measured. In total, 95 sets of data are collected for evaluation. As the phase shift caused by the fluid

is determined by both the conductivity of the fluid and the volume of the fluid, the phase shift varies accordingly. Fig. 10 shows the norm value of the phase difference against the volume of fluid, when the total volume of the fluid increases from 4 to 15 litres at five different conductivity values. There is an increase in the norm value when the fluid begins to reach the bottom of the coil array, and as the volume of the fluid increases, the norm value decreases. Further increases in the volume result in consistent increases in the norm value of the phase difference, with eventual saturation of the phase perturbation after 12 litres of fluid.

The fluid reaches the centre of the imaging region when the flow rig is filled with 9 litres of fluid. Fig. 11 shows the norm value of the phase difference for five different conductivity backgrounds
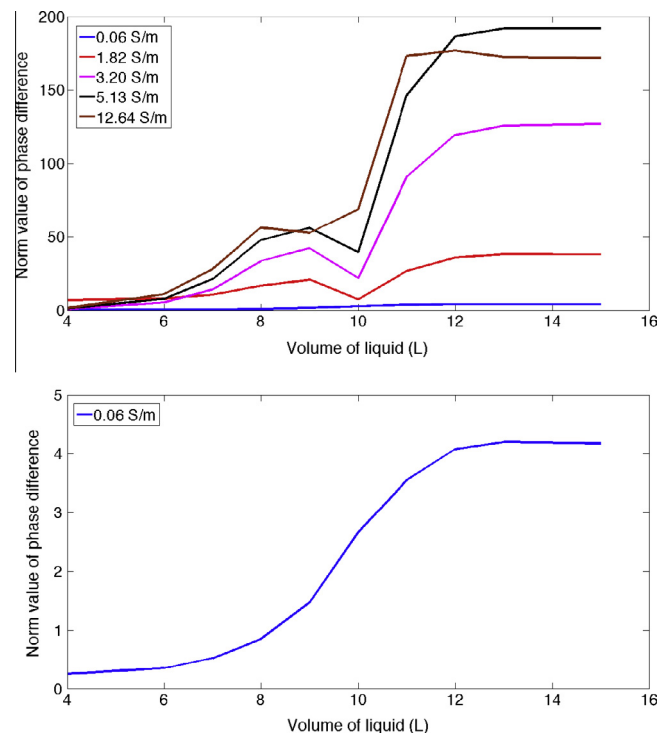
Fig. 10. The norm value of the phase difference against the volume of the fluid for backgrounds with five different conductivities (top). Shown in blue, red, magenta, black, and brown are conductivities of 0.06 S/m, 1.81 S/m, 3.20 S/m, 5.13 S/m and 12.64 S/m respectively. The norm value of the phase difference against the volume of the fluid for a tap water background is shown in the bottom half of the figure. (For interpretation of the references to colour in this figure legend, the reader is referred to the web version of this article.)
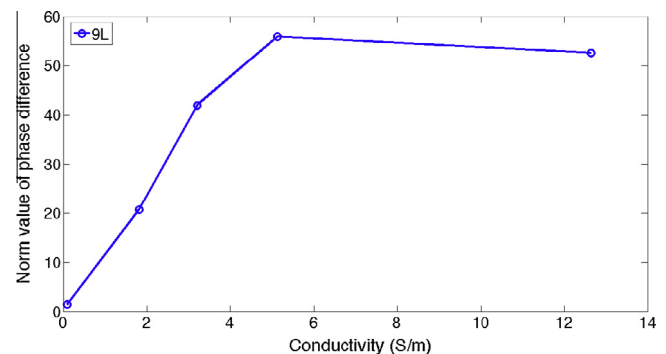
Fig. 11. The norm value of the phase difference for five difference conductivity backgrounds (0.06 S/m, 1.81 S/m, 3.20 S/m, 5.13 S/m and 12.64 S/m respectively) when the flow rig is filled with 9 litres of fluid.

when the flow rig is filled with 9 litres of fluid. There is a consistent increase in the norm value as the conductivity increases, which reaches its peak value at a conductivity of 5.13 S/m.

Once the flow rig is filled with 15 litres of fluid, a stream of bubble gas is injected on the periphery at 2 points opposite each other (labelled position 1 and position 2 in Fig. 12) to introduce the perturbation to the electromagnetic field. The aim of the experiment is to test whether the system can reconstruct an image of the bubbles. A snap shot of the bubble testing is reconstructed to show the average bubbles along the axial direction. The imaging results are shown in Fig. 12; note the value of the scale decreases as the conductivity of the background decreases. Although the gas bubbles are themselves non-conductive, they are injected into a conductive background; as such, the areas that are injected with gas bubbles in fact have a non-homogenous non-conductive feature. This experiment can be considered the opposite of the experiment shown in Fig. 8, where the results show the reconstructed images of a non-homogenous conductive medium in a non-conductive background.

Fig. 13 shows the experimental setup and the reconstructed images of silicone oil within a saline solution. The silicone oil is bottled in a non-conductive container of height 180 mm and outer diameter 130 mm. The basal position of the container is initially placed at the bottom of the flow rig and raised by 5 cm until it surpasses the fluid level. The experiment is performed twice, with a background conductivity of 1.81 S/m and 12.64 S/m respectively.

Fig. 14 shows the norm value for the phase difference resulting from the movement of the silicone oil along the axial direction within the conductive background. The distance whereby the silicone oil container is placed within the imaging region is set to be the reference distance, i.e., 0 cm along the axial direction. For a background with 1.81 S/m conductivity, the norm value of the phase difference initially decreases; from −15 cm and greater, however, the value starts to increase. This is also called the fringe effect of the sensing region as the sensing area in the axial direction depends on the conductivity contrast between the background and the inclusion (Sun and Yang, 2013), consistent with the observations in Fig. 10. The norm value of the phase difference reaches its peak when the silicone oil container arrives in the imaging region. Further increasing the distance, the value starts to decrease again. As the distance surpasses 15 cm, the silicone oil does not seem to cause any distinct perturbation in the phase difference. For the background with conductivity 12.64 S/m, the overall norm value of the phase difference does not change as sharply as that for 1.81 S/m. At −20 cm, the norm value of the phase difference caused by background conductivities of 1.81 S/m and 12.64 S/m are 10.94 and 12.83 respectively. As the norm value of the phase difference caused by a higher conductive background already exceeds its counterpart, at this point, the fringe effect is not observed between −20 to −10 cm.

Discussion

The visualisation of conductive phase flow is a challenging problem in industrial process tomography, with a need to develop a cost-effective, non-invasive yet robust imaging technique in this area. This paper investigates the feasibility of MIT for this application and also highlights the difficulties associated with it. Four background measurements are collected by contrasting both
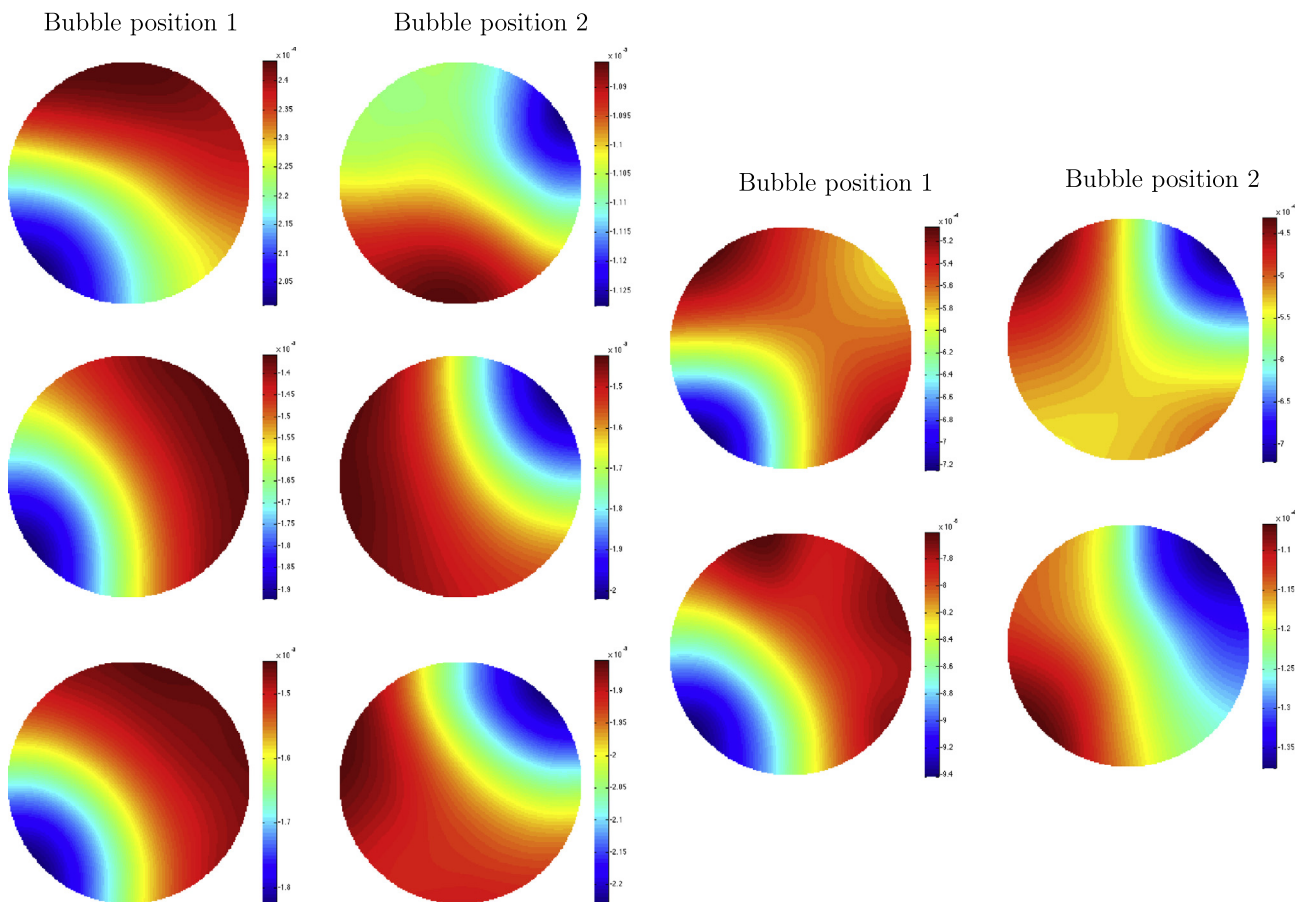

Fig. 12. Reconstructed images of bubble flow in various backgrounds. Background conductivities are, by row, 12.64 S/m, 5.13 S/m, 3.20 S/m, 1.81 S/m and 0.06 S/m respectively.
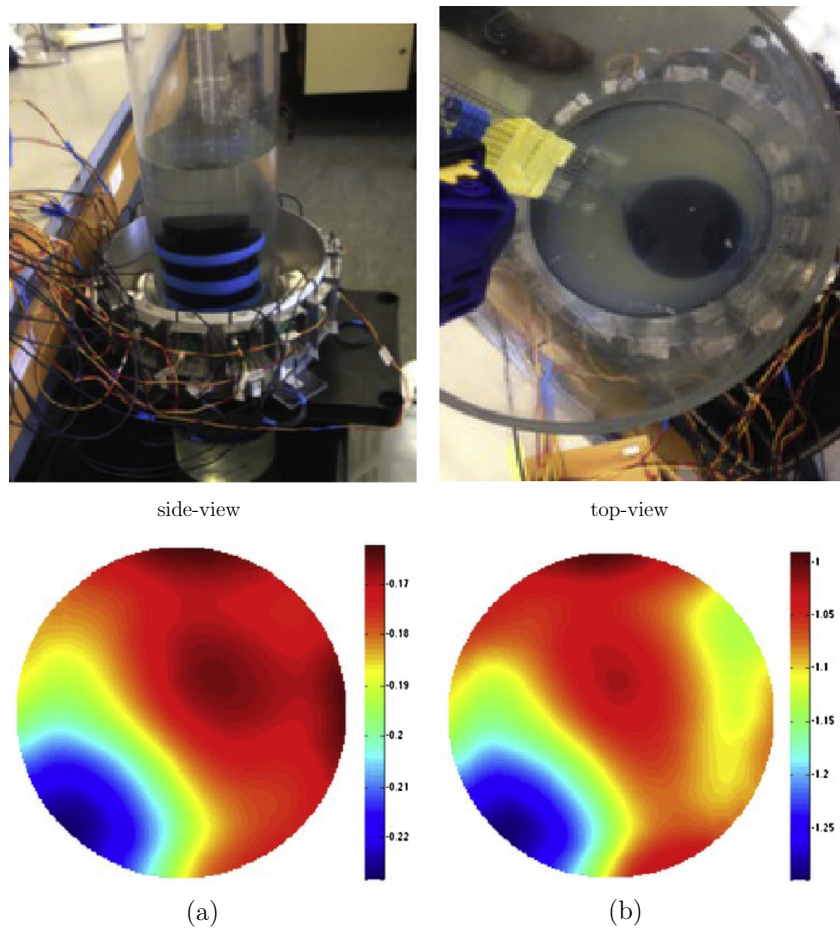
Fig. 13. Experimental setup of a silicone oil inclusion in two conductive backgrounds, with associated images. (a) silicone oil inclusion within a 1.81 S/m background, (b) silicone oil inclusion within a 12.64 S/m background.
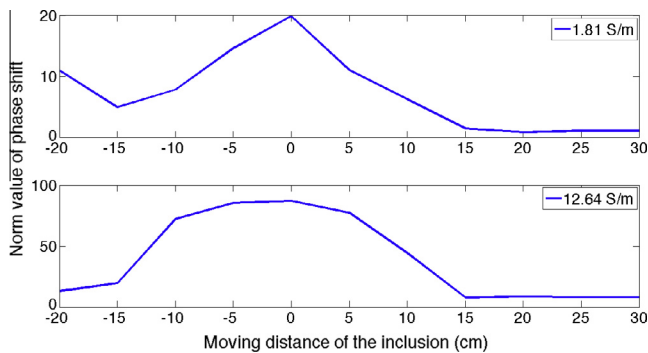

Fig. 14. The norm value of the phase difference resulting from the movement of the silicone oil along the axial direction within two conductive backgrounds, 1.81 S/m and 12.64 S/m respectively.

non-conductive (free space and silicone oil) and conductive fluids (saline solution and tap water, with conductivities of 1.52 S/m and 0.06 S/m, respectively) to represent a range of scenarios of potential interest in industrial process tomography. The results of static fluid tests confirm the viability of MIT in visualising the conductivity contrasts. We also found that the MIT phase measurements show a linear response with respect to electrical conductivity for a given dimension and location of an inclusion, while the phase changes arising from the changing dimensions of an inclusion have a non-linear relationship.

In addition, it is commonplace to have fluids separated into different layers by density, weight or conductivity in industrial process tomography. Tests of non-homogenous conductive fluids suggest that different strata of conductive fluids can be distinguished, and although in this case the distribution of eddy currents could differ from an industrial flow environment, we nevertheless show the potential of MIT in this respect. In industrial environments, there may be bubble flows of gas in the uppermost part of the flow pipe, and water only in the lowest part. The quasi-static experiments demonstrate the capability of MIT in obtaining a 2D image of bubble flow along the axial dimension of various conductive backgrounds, including water.

These quasi-static experiments also reveal that there is a strong fringing field effect of the MIT sensing region, consistent with similar observations in (Vauhkonen et al., 2007). This suggests that a 3D MIT system might be more robust compared to a 2D system, particularly in obtaining the axial information of the fluid. Future studies will focus on this aspect with the purpose to design a cost effective 3D system, and subsequently develop real time 3D reconstruction algorithms. For any conductivity contrast lower than the conductivity contrast presented in this study, other contactless imaging techniques such as electrical capacitance tomography might be able to operate. A combined capacitance and inductive tomographic system will be studied in order to image both dielectric and conductive phase contrasts. In our continued effort, we will develop a more robust MIT hardware capable of working in industrial environments, including both the mechanical design of the sensors and improvement in hardware electronics.

Finally, it is worth mentioning that in principle, the inverse problem needs to be solved according to each specific imaging case. As such, the image reconstruction algorithm needs to be applied according to each individual imaging subject. This would introduce additional parameters (i.e., the number of iterations, the regularisation parameters or matrices) to this study, alongside the number, size and position of inclusions, and the conductivity contrast. Therefore, in this study, a universal linear inverse algorithm is used to reconstruct images with pre-calculated regularisation parameters for all cases. This way, it is guaranteed that any change in the image reconstruction is in fact due to the change in the fluid distribution patterns rather than the image reconstruction software model, although this does suggest that the inverse model might not be optimal for certain cases. In this study, a time difference imaging model is used in all reconstructed images, which means the image represents a change in the conductivity value and the colour bar correlates with the level of conductivity change. For instance, if the conductivity of an inclusion is lower than the background conductivity, a negative conductivity change is shown in blue colour; on the contrary, if the conductivity of an inclusion is higher than the background conductivity, a positive conductivity change is shown in red colour. In future studies, a nonlinear image reconstruction algorithm might be necessary to enhance the resolution of the two phase contrasts, if it can be developed in such a manner as to computationally efficient for the purpose of real time imaging.

Conclusion

This study presents an experimental evaluation of MIT in conductive phase flow imaging. Experiments are conducted covering as broad a range of conductivity contrasts as possible, so as to encompass several scenarios of potential interest in industrial flow environments. Our evaluation of fluid experiments includes (a) a range of conductivity contrasts in which image reconstruction in various non-conductive and conductive backgrounds is possible, (b) distinguishing three distributions of non-homogenous conductive fluids in a free space, and (c) imaging a flow of non-homogenous bubbles of gas in various conductive backgrounds. Taken together, we demonstrate various capabilities of an MIT system in conductive phase imaging. With continued effort in both hardware and software development, MIT could eventually evolve to become a low cost, non-invasive and fast imaging device in multiphase flow tomography.

References

Albrechtsen, R.A., Yu, Z.Z., Peyton, A.J., 1995. Preliminary experiments on the investigation of the inductive technique for measuring water content in multiphase flow. In: Proc. ECAPT, Bergen, pp. 205–213.

AL-Zeibak, S., Saunders, N.H., 1993. A feasible study of in vivo electromagnetic imaging. Phys. Med. Biol. 38, 151–160.

Biro, O., 1999. Edge element formulations of eddy current problems. Comput. Methods Appl. Mech. Eng. 169, 391–405.

Chen, Z., Lu, Y., Xu, Y., Yang, H., 2008. Multi-parameter tikhonov regularization for linear ill-posed operator equations. J. Comput. Math. 26, 37–55.

Daily, W., Ramirez, A., 1995. Environmental process tomography in the United States. Chem. Eng. J. Biochem. Eng. J. 56, 159–165.

Griffiths, H., 2001. Magnetic induction tomography. Measure. Sci. Technol. 12, 1126–1131.

Griffiths, H., Stewart, W.R., Gough, W., 1999. Magnetic induction tomography: a measuring system for biological tissues. Ann. New York Acad. Sci. 873, 335–345.

Hammer, E.A., Fossdal, G., 2002. A new water-in-oil monitor based on high frequency magnetic field excitation. In: Proceedings of the 2nd International Symposium on Process Tomography, Wroclaw, Poland, pp. 9–16.

Hu, L., Wang, H.X., Zhao, B., Yang, W.Q., 2007. A hybrid reconstruction algorithm for electrical impedance tomography. Measure. Sci. Technol. 18, 813–818.

Igney, C.H., Watson, S., Williams, R.J., Griffiths, H., Dossel, O., 2005. Design and performance of a planar-array mit system with normal sensor alignment. Physiol. Measure. 26, S263–S278.

Jin, H., Lian, Y., Yang, S., He, G., Guo, Z., 2013. The parameters measurement of air-water two phase flow using the electrical resistance tomography (ERT) technique in a bubble column. Flow Measure. Instrum. 31, 55–60.

Karbeyaz, B.U., Gencer, N.G., 2003. Electrical conductivity imaging via contactless measurements: an experimental study. IEEE Trans. Med. Imaging 22, 627–635.

Korzhenevsky, A.V., Sapetsky, S.A., 2001. Visualization of the internal structure of extended conducting objects by magnetoinduction tomography, magnetoinduction tomography bull. Russian Acad. Sci. Phys. 65, 1945–1949.

Liu, Z., He, M., Xiong, H.-L., 2005. Simulation study of the sensing field in electromagnetic tomography for two-phase flow measurement. Flow Measure. Instrum. 16, 199–204.

Lu, S., Pereverzev, S.V., Tautenhahn, U., 2008. Dual regularized total least squares and multi-parameter regularization. Comput. Methods Appl. Math. 8, 253–262.

Ma, L., Soleimani, M., 2012. Electromagnetic imaging for internal and external inspection of metallic pipes. Insight-Non-Destruct. Test. Cond. Monit. 54, 493–495.

Ma, X., Peyton, A.J., Higson, S.R., Lyons, A., Dickinson, S.J., 2006. Hardware and software design for an electromagnetic induction tomography (emt) system for high contrast metal process applications. Measure. Sci. Technol. 17, 111–118.

Ma, X., Peyton, A.J., Higson, S.R., Drake, P., 2008. Development of multiple frequency electromagnetic induction systems for steel flow visualization. Measure. Sci. Technol. 19.

Ma, L., Wei, H.-Y., Soleimani, M., 2012. Cryosurgical monitoring using electromagnetic measurements: a feasibility study for magnetic induction tomography. In: 13th International Conference in Electrical Impedance Tomography, 2012-05-23 – 2012-05-25, Tianjin University, Tianjin.

Peyton, A.J., Mackin, R., Goss, D., Wan-daud, W.A., Crescenzo, E., Saunders, N.H., Tapp, H.S., 2003. Addressing the difficulties in using inductive methods to evaluating human body compositions. Biomet. Hum. Anthropol. 21, 69–77.

Renner, A., Fischer, H.-J., Marschner, U., 2012. A new imaging approach for in-situ and ex-situ inspections of conductive fiber reinforced composites by magnetic induction tomography (mit). J. Intell. Mater. Syst. Struct., 897–902

Rosell-Ferrer, J., Merwa, R., Brunner, P., Scharfetter, H., 2006. A multifrequency magnetic induction tomography system using planar gradiometers: data collection and calibration. Physiol. Measure. 27, S271–S280.

Scharfetter, H., Lackner, H.K., Rosell, J., 2001. Magnetic induction tomography: hardware for multi-frequency in biological tissue. Physiol. Measure. 22, 131–146.

Soleimani, M., 2006. Sensitivity maps in three-dimensional magnetic induction tomography. Insight: Non-Destruct. Test. Cond. Monit. 48, 39–44.

Soleimani, M., Lionheart, W.R.B., 2006. Absolute conductivity reconstruction in magnetic induction tomography using a nonlinear method. IEEE Trans. Med. Imaging 25, 1521–1530.

Su, L., Song, Z.-P., Wang, B.-S., Ding, L., 2013. Research on void fraction of gas-liquid two-phase flow based on comsol and matlab. J. Ship Mech. 17, 460–467.

Sun, J.T., Yang, W.Q., 2013. Fringe effect of electrical capacitance and resistance tomography sensors. Measure. Sci. Technol. 24, 074002.

Terzija, N., Yin, W., Gerbeth, G., Stefani, F., Timmel, K., Wondrak, T., Peyton, A.J., 2011. Use of electromagnetic induction tomography for monitoring liquid metal/gas flow regime on a model of an industrial steel caster. Measure. Sci. Technol. 22, 015501.

Thorn, R., Johansen, G.A., Hjertaker, B.T., 2013. Three-phase flow measurement in the petroleum industry. Measure. Sci. Technol. 24, 012003.

Vauhkonen, M., Hamsch, M., Igney, C.H., 2007. Image reconstruction approaches for philips magnetic induction tomograph. In: IFMBE Proceedings: 13th International Conference on Electrical Bioimpedance and the 8th Conference on Electrical Impedance Tomography, vol. 17.

Watson, S., Morris, A., Williams, R.J., Gough, W., Griffiths, H., 2002. The cardiff magnetic induction tomography system. In: Proceedings of the International Federation for Medical and Biological Engineering EMBEC'02 Part 1, December 04–08, Vienna, Austria, p. 116.

Watson, S., Williams, R.J., Gough, W., Griffiths, H., 2008. A magnetic induction tomography system for samples with conductivities below 10 s/m. Measure. Sci. Technol. 19, 045501.

Wei, H.Y., Soleimani, M., 2012. Two-phase low conductivity flow imaging using magnetic induction tomography. Prog. Electromagnet. Res. (PIER) 131, 97–115.

Wei, H.Y., Soleimani, M., 2012. Hardware and software design for a national instrument-based magnetic induction tomography system for prospective biomedical applications. Physiol. Measure. 33, 863–879.

Widlak, T., Scherzer, O., 2012. Hybrid tomography for conductivity imaging. Inverse Problems 28, 084008.

Yin, W., Peyton, A.J., 2006. A planar emt system for the detection of faults on thin metallic plates. Physiol. Measure. 17, 2130–2135.

Zhang, J., Ma, F., 2013. Application of electrical resistance tomography to ice-water two-phase flow parameters measurement. Key Eng. Mater. 562–565, 686–690.

Zhang, M., Ma, L., Soleimani, M., 2014. Magnetic induction tomography guided electrical capacitance tomography imaging with grounded conductors. Measurement 53, 171–181.